# A methodology for understanding phase-contrast tomography

**Preveshin Maduray[1], Timothy Brooks[2], Simon Connell[2], Charis Harley[1], Neil Martinson[3], Threnesan Naidoo[4], Adrie Steyn[4] and Gordon Wells[4]**

[1]Electrical and Electronic Engineering Science, University of Johannesburg, Johannesburg, South Africa
[2]Mechanical Engineering Science, University of Johannesburg, Johannesburg, South Africa
[3]Perinatal and HIV Research Unit, University of Witwatersrand, Johannesburg, South Africa
[4]Africa Health Research Unit, University of Kwa-Zulu-Natal, Durban, South Africa

E-mail: preveshinm@uj.ac.za

**Abstract.** Artificial Intelligence (AI) classification as a methodology and approach to identify Tuberculosis (TB) in patients has become a topic of increasing interest in the past few decades. This is in large part due to the increasing demand for faster methods of detecting TB to reduce spread. However, such methodologies require large datasets so that algorithms can learn the manifestations of TB in the lung. Some of these datasets are private due to patient confidentiality, and the publicly available ones are limited in number. The AI industry has exhausted publicly available chest X-ray (CXR) scans and now look for alternate methods to further develop research in the field. The study focuses on developing methods to translate 3D information on effective electron density from Hierarchical Phase Contrast tomography (HiP-CT) of a human lung to 3D segmented images based on differentiated effective atomic number and mass density. The purpose of this methodology is to create a digital phantom as a synthetic model of a human lung where pathologies of the various stages of TB can be inserted. Monte Carlo modeling of X-ray radiography can then be performed on sets of such digital phantoms to produce a library of 2D conventional X-ray radiographs labeled with details of the occurrence of TB pathologies. This synthetic data set can be used to train an AI classifier. The study will leverage HiP-CT scans produced by the European Synchrotron Research Facility (ESRF) beamline BM18. These are high-resolution 3D scans of complete human organs. To create a synthetic dataset, the Geant4 toolkit will be used to simulate labeled 2D X-ray radiographs starting from the properties and physiological conditions of a lung. This information is gathered from the HiP-CT images; to understand the material properties of the HiP-CT images, the phase shift ($\delta$) and the effective mass densities ($\rho_{eff}$) of the organic materials within the lung must be known. Thus, this research builds on the derivation of equations and the calculation of these parameters as inputs for simulation and describes our workflow towards the synthetic images.

## 1 Introduction

Tuberculosis (TB) is a significant global health crisis facing many countries and one of the leading causes of death from a single infectious disease [1]. Through early detection, the disease can be cured and the spread contained. A chest radiograph allows experienced physicians to identify the early presence of TB. However, the process requires a keen eye and an experienced professional in the field of radiography, where some cases may lead to inconsistent diagnostics due to poor imaging contrast.

To reduce/mitigate false diagnosis, AI tools are leveraged to assist in TB detection. These solutions are based on machine learning (ML) algorithms that assist in identifying the different ways TB manifests from Chest X-Rays (CXR) of diagnosed patients. For an ML algorithm to detect TB from a CXR, a repository of CXR data (preferably labeled) is required for the algorithm to learn how TB presents in the lung. The size of the dataset required in order to ensure that the algorithm is trained properly is often found to be quite large, which can hinder progress in the field.

The comparative study covered in [2] investigates different ML techniques used for TB detection. The study, in addition, outlines the different datasets used to train and test the accuracy of the algorithms. An important aspect of the study covered in [2] which forms the foundation for the research covered in this study, is the overuse of publicly available CXR datasets. Due to privacy constraints, the only available CXR datasets are those made available to the public; researchers have exhausted the use of these datasets to the point of testing algorithms on the same data on which they were trained. This process is repeated for each "improved" technique used for detection, inevitably increasing the accuracy in detection.

The purpose of the conducted study is to create a computationally simulated 3D healthly lung model that can be modified in a stochastic way to demonstrate the different manifestations of TB at different locations, following the natural physiological conditions of a diseased human lung. The aim is to create a labeled dataset of CXR images of healthy and TB infected lungs that can be used to train ML algorithms for TB detection. This process introduces new CXR data to the public and allows the manipulation of the model to suit different pathologies according to the different stages TB manifests in the lung. This introduces a dataset that has never been explored nor published in existing literature.

The study will leverage 3D scanned digital human lung datasets from the ESRF, scanned from beamline 18 (BM18) using Hierarchical Phase-Contrast Tomography (HiP-CT). With these datasets, the aim is to translate the 3D information of the effective electron density $\rho_{eff}$ from the HiP-CT of the organ into 3D segmented images based on the differentiated effective atomic number $Z_{eff}$ and mass density $\rho_{mass}$.

The translation of information from the HiP-CT dataset to a material composition format will be done as an additional data preparation step before including it into the Geant4 toolkit. Geant4 will then be used to model the X-ray particle transport through the lung to the detector forming the usual 2D X-ray absorption contrast radiographs. This software leverages Monte Carlo modeling of random particle interactions with matter to create a 2D conventional X-ray radiograph image with labeled TB pathologies.

## 2 Basic Physical Principles and Theorems

### *2.1 Particle Interaction in X-ray Diagnostics*

In x-ray diagnostics, the linear attenuation of a material at a specified energy $E$ is separable into two parts; the contributions from the photoelectric cross-section $\sigma_{PE}$ and the scattering cross-section $\sigma_{SC}$ [3]. The relationship of the attenuation coefficient and the two components at the beam energy $E$, can be expressed as,

$$\mu = \rho_{mass} \frac{N_A}{A_{mass}} (\sigma_{PE}(E) + \sigma_{SC}(E)) \tag{1}$$

where $\rho_{mass}$ is the mass density of the material, $N_A$ is Avogadro's constant ($N_A$ = $6.022 \times 10^{23}\text{mol}^{-1}$) and $A_{mass}$ represents the atomic mass of a material.

According to [3], the cross-sections $\sigma_{PE}$ and $\sigma_{SC}$ can be given by the following formulas, where $\sigma_{SC}$ can be described as a combination of Compton scattering and coherent scattering cross-sections,

$$\sigma_{PE}(E) \sim K \frac{Z^m}{E^3} \tag{2}$$

where $K$ is a constant and $Z^m$ is the effective atomic number of a material raised to a constant [3].

$$\sigma_{SC}(E) = Z[\phi_{\text{KN}}(E) + \phi_{\text{coh}}(Z, E)] \tag{3}$$

where $\phi_{\text{KN}}(E)$ represents the Klein-Nishina cross-section and $\phi_{\text{coh}}(Z, E)$ represents the coherent scattering cross-section. However, the contribution of the coherent scattering cross-section of the X-ray is negligible and thus, using the expression of the electron density expressed as a function of the linear attenuation $\mu$ [3],

$$\mu = \rho_e \left[ \frac{\phi_{PE}(E)}{Z} + \phi_{\text{KN}}(E) \right] \tag{4}$$

equation (4) can be rewritten as,

$$\mu = \rho_e [K \frac{Z^{m-1}}{E^3} + \phi_{\text{KN}}(E)] \tag{5}$$

Recall that the Compton scattering cross-section was derived from the Klein-Nishina formula equation (4). Here, Compton scattering is divided into two parts; the Compton scattered ($\sigma_{scatt}$) and Compton absorption ($\sigma_{absp}$).

$$\sigma_c = 2\pi {r^2}_e \{ \frac{1+\gamma}{\gamma^2} [ \frac{2(1+\gamma)}{1+2\gamma} - \frac{1}{\gamma} ln(1+2\gamma)] + \frac{1}{2\gamma} ln(1+2\gamma) - \frac{1+3\gamma}{(1+2\gamma)^2} \} \tag{6}$$

At X-ray energies, the low energy limit, the Compton absorption becomes small, and the Compton cross-section becomes,

$$\sigma_c = 2\pi {r^2}_e [1] \tag{7}$$

Therefore,

$$\phi_{\text{KN}}(E) \equiv \sigma_c = 2\pi {r^2}_e [1] \tag{8}$$

The dependence of the photo-electric cross section on the atomic number of the material is $Z^5$. However the dependence of the Compton scattering cross section is $Z^1$, as the equation (8) is on a per electron basis. If both processes occur together in a compound or mixture, then it will lead to an effective $Z$ as discussed in the next section.

### *2.2 Mass Density Derivation*

X-ray computed tomography (CT) is an imaging technique based on principles discussed above. The normal implementation uses absorption contrast radiography to produce the 2D X-ray images that are tomographically combined into a 3D image [3]. It is also possible to base the tomography on X ray phase contrast imaging, as in the HiP-CT technique described above. The refractive index of a material can be defined by the equation $n = 1 - \delta + i\beta$ where $\delta$ represents the real part of the refractive index and $\beta$ its imaginary part. The real part, $\delta$ is responsible for the phase contrast and the imaginary part, $\beta$ is responsible for the absorption contrast. The attenuation of the transmitted X-ray is proportional to $\mu = 4\pi\lambda^{-1}\beta$ [3]. The real part $\delta$ is related to the imaginary part via the Kramers-Kronig relations. At X-ray energies, the real part is typically three to four orders of magnitude larger than the imaginary part. Therefore for X ray Tomography, phase contrast imaging will typically display much higher sensitivity to small variations in material composition and density, and have a much higher dynamical range. Phase contrast imaging has become the preferred technique at synchrotron light sources.

The phase shift $\delta$ demonstrates a proportional relationship with the electron density $\rho_e$ of a material and an inverse relationship with the incident beam energy $E$ [3],

$$\delta = \frac{\rho_e r_e \hbar^2 c^2}{2\pi E^2} \tag{9}$$

where $r_e$ represents the classical radius of an electron $r_0$=2.82 x $10^{-15}$ m, $\hbar$ is the reduced Planck's constant and $c$ is the speed of light. In reference [3], an equation representing the effective atomic number $Z_{eff}$ for a mixture of several elements each with a different $Z$ is derived,

$$Z_{eff} = \sqrt[k]{\sum_i f_i (Z_i)^k} \tag{10}$$

where $f_i$ represents the total number of electrons associated with each element in a compound and $Z_i$ is the atomic number of the elements. In reference [4], $k$ is defined by the parametrization of the Z-dependence at high photon energies, and is defined by $k = B(E)lnZ + C(E)$ [4]. However, in reference [5], $k$ is defined as 2.94 for biological specimens. One notes that this is intermediate between the $Z^5$ and $Z^1$ atomic number dependence of the photo-electric effect and the Compton effect respectively.

According to [3], the effective electron density can be defined as follows,

$$\rho_{eff} = \frac{\rho_{mass} N_A Z_{eff}}{A_{mass}} \tag{11}$$

Furthermore, the effective electron density $\rho_{eff}$ can be calculated as a function of the effective atomic number ($Z_{eff}$),

$$\rho_{eff} = \frac{\rho_{mass} N_A \sqrt[k]{\sum_i f_i (Z_i)^k}}{A_{mass}} \tag{12}$$

To calculate the phase shift for a material, substitute equation (12) in (9), the following is derived;

$$\delta = \frac{[\rho_{mass} N_A \sqrt[k]{\sum_i f_i (Z_i)^k}] r_e \hbar^2 c^2}{2\pi E^2 A_{mass}} \tag{13}$$

Equation (13), describes the proportionality between the phase shift ($\delta$) and the effective electron density ($\rho_{eff}$) of a material expressed as a product of the effective atomic number ($Z_{eff}$) and the mass density ($\rho_{mass}$).

The term "effective" associated with the atomic number and electron density is derived from the average of the Z-dependence with different exponents and two or more elements in a compound. Thus, in this case an assumption is made where the value of $k$ is a substitute for biological materials. A key point from equation 13 is that a 3D HiP-CT digital image is quantitative in the effective electron density $\delta$.

## 3 Discussion

The figure below is a healthy lung sample scanned at the ESRF using HiP-CT at a resolution of $100\,\mu\mathrm{m}$. Identifying the different organic materials present in the data set is a challenge.

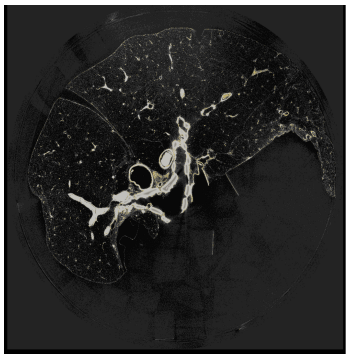

Figure 1: Healthy lung lobe scanned at the ESRF using HiP-CT. The grey scale is proportional to the effective electron density $\delta$ using the equation from equation 13 and the know compositions of these materials.

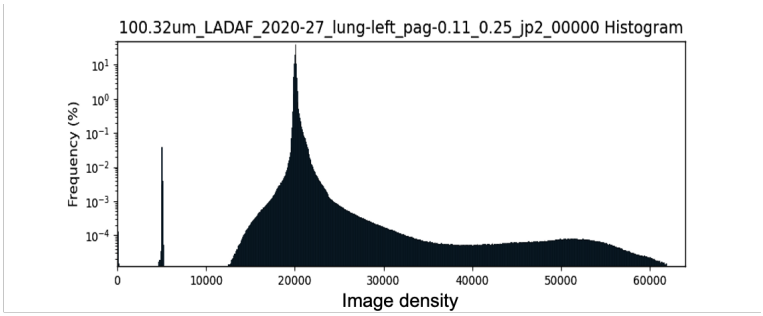


Figure 2: Image Threshold for Segmentation. The x-axis is currently a 2 byte integer. It is proportional to the effective electron density $\delta$.

Figure 2, represents the image histogram, this identifies a number proportional to the effective electron density per voxel. The range provides information on the number of different organic materials present in figure 1 by the density of the compound. Certain materials, such as the voids which are inflated with formalin and the blocks of agar, can be used to calibrate the effective electron density, as the elemental composition of these materials is known.

The image segmentation performed on the dataset aids in understanding the organic material present and assists with differentiating between the organ material and the supporting structures. Understanding the effective electron densities of all materials in the dataset allows the segmentation of the lung structure into specific materials. These can then be mapped into the lung structure in terms of a material composition and a density, such that the correct effective density is achieved. This is then the final 3D model including a description of geometry and materials that is used in building a simulation of the lung model in Geant4.

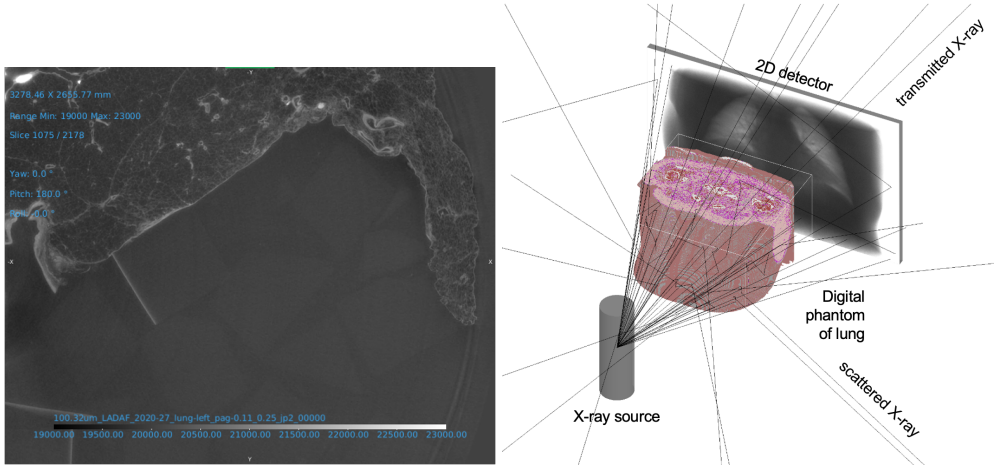


Figure 3: (*left*) Segmentation Based on Threshold. (*right*) and Geant4 Simulation Construction

The image on the right of figure 3 is an illustration of the simulation setup in the Geant4 environment. By understanding the effective properties of materials, the interaction between photons and the materials, this will produce the scattered and transmitted X-rays, where the transmitted X-rays would be reconstructed into a simulated CXR with TB manifestations according to the digital phantom.

Using equations (12) and (13) will assist in calculating the effective properties of the organic compounds from the HiP-CT dataset and their phase shifts. For a given $A_{mass}$, $k$ and $\rho_{mass}$, the following table represents the calculated $Z_{eff}$, $\rho_{eff}$ and $\delta$ for different materials that can be found within the dataset.

| Material | $A_{mass}$ (g/mol) | $k$ | $\rho_{mass}$ (g/$cm^3$) | $Z_{eff}$ | $\rho_{eff}$ ($e/cm^3$) | $\delta$ |
|---|---|---|---|---|---|---|
| water | 18 | 2.94 | 1 | 5.50 | 1.84x$10^{23}$ | 3.57x$10^{-9}$ |
| formalin | 20 | 2.94 | 1.09 | 6.99 | 2.29x$10^{23}$ | 4.45x$10^{-9}$ |
| ethanol | 24 | 2.94 | 0.789 | 6.62 | 1.31x$10^{23}$ | 2.54x$10^{-9}$ |
| protein | 22 | 2.94 | 1.35 | 6.63 | 2.45x$10^{23}$ | 4.75x$10^{-9}$ |
| fat | 26 | 2.94 | 0.92 | 6.59 | 1.40x$10^{23}$ | 2.72x$10^{-9}$ |
| carbohydrate | 24 | 2.94 | 1.5 | 7.25 | 2.73x$10^{23}$ | 5.30x$10^{-9}$ |
| bone | 20 | 2.94 | 1.85 | 13.39 | 7.40x$10^{23}$ | 1.44x$10^{-8}$ |
| agar | 13.35 | 2.94 | 1.032 | 7.16 | 3.33x$10^{23}$ | 6.47x$10^{-9}$ |

Table 1: Table representing Atomic Mass Number ($A_{mass}$), Parametrization Dependence ($k$), Mass Density ($\rho_{mass}$), Effective Atomic Number ($Z_{eff}$), Effective Electron Density ($\rho_{eff}$) and Phase Shift ($\delta$) of several materials.

The range of $A_{mass}$ and $\rho_{mass}$ for protein, fat, carbohydrates and bone is specific to a general composition of compounds found in lung tissue and the chest cavity. For water, formalin, ethanol and agar, this is specific to the procedure for scanning in a HiP-CT application.

Table 1 represents a quantitative value for different materials that can be present in a HiP-CT dataset. Water was selected due to the possibility of trace compounds present in the lung or on the surface; formalin and ethanol were selected as the organ is submerged into a preserving fluid that is a combination of the two materials. Proteins, fat, and carbohydrates were selected as these compounds are the main constituents of organ tissue in varying percentages according to tissue type and function. Bone was selected however, no bone material is present in the dataset but understanding the effective electron density is important since a 2D CXR would include the entirety of the chest cavity, including bone material. Agar was selected as it is the material used to maintain the upright structure of the organ during scanning and is quite distinguishable in the left image of figure 3.

## 4 Conclusion

The research proposes a novel technique for creating a labeled synthetic data set of CXR absorption radiographs that can be used in many different applications. The technique leverages high-resolution HiP-CT 3D imaging to create 2D radiographs. This requires an understanding of how to extract material quantities based on effecive electron density as appropriate for a phase contrast a high-resolution HiP-CT dataset and then how to use this information to create a low-resolution 2D absorption contrast radiographic image.

The HiP-CT dataset contains the effective electron density information, and by performing a threshold-based segmentation one can separate the different materials present in the dataset to identify the structure of the organ and separate the tissue compounds. The segmentation technique identifies the material present in the image on a per voxel basis. Given an $A_{mass}$ and $\rho_{mass}$ for a biological constant $k$, using equation (12) and equation (13), the $\rho_{eff}$ and $\delta$ for a specific compound can be calculated. This aligns a quantitative value to a material compound.

The quantitative information is captured in Geant4. The pathologies can be inserted in healthy tissue in a stochastic way so that a synthetic model made of known materials and associated densities can be simulated. In this manner, TB pathologies can be introduced into the model to create a labeled digital phantom and 2D radiographs can be captured.

This method introduces a new approach for generating a synthetic dataset of labeled pathologies and introduces the prospect of creating images that can demonstrate more than one pathology. In this manner, we aim to build an AI classification tool that has been trained on a multitude of ways the disease can present itself.

## References


[1] N. Pattamapaspong, T. Kanthawang, W. C. G. Peh, N. Hammami, M. C. Bouaziz, and M. F. Ladeb, "Imaging of thoracic tuberculosis: pulmonary and extrapulmonary," *BJR|Open*, vol. 6, no. 1, p. tzae031, 09 2024.

[2] R. S. Prasad, R. C. Waghmare, T. B. Pajgade, R. R. Raut, and M. L. Mahajan, "A comparative study of detection of tuberculosis using machine learning & deep learning," in *2023 10th International Conference on Computing for Sustainable Global Development (INDIACom)*, 2023, pp. 1217–1221.

[3] Z. Qi, J. Zambelli, N. Bevins, and G.-H. Chen, "Quantitative imaging of electron density and effective atomic number using phase contrast CT," *Physics in medicine and biology*, vol. 55, pp. 2669–77, 05 2010.

[4] W. Langeveld, "Effective atomic number, mass attenuation coefficient parameterization, and implications for high-energy x-ray cargo inspection systems," *Physics Procedia*, vol. 90, pp. 291–304, 12 2017.

[5] R. C. Murty, "Effective Atomic Numbers of Heterogeneous Materials," *Nature*, vol. 207, no. 4995, pp. 398–399, Jul. 1965.